



HAL
open science

Search for the Standard Model Higgs boson e^+e^- collisions at \sqrt{s} up to 202 GeV

M. Acciarri, P. Achard, O. Adriani, M. Aguilar-Benitez, J. Alcaraz, G. Alemanni, J. Allaby, A. Aloisio, M.G. Alviggi, G. Ambrosi, et al.

► **To cite this version:**

M. Acciarri, P. Achard, O. Adriani, M. Aguilar-Benitez, J. Alcaraz, et al.. Search for the Standard Model Higgs boson e^+e^- collisions at \sqrt{s} up to 202 GeV. Physics Letters B, 2001, 508, pp.225-236. 10.1016/S0370-2693(01)00326-4 . in2p3-00009822

HAL Id: in2p3-00009822

<https://in2p3.hal.science/in2p3-00009822v1>

Submitted on 13 Dec 2001

HAL is a multi-disciplinary open access archive for the deposit and dissemination of scientific research documents, whether they are published or not. The documents may come from teaching and research institutions in France or abroad, or from public or private research centers.

L'archive ouverte pluridisciplinaire **HAL**, est destinée au dépôt et à la diffusion de documents scientifiques de niveau recherche, publiés ou non, émanant des établissements d'enseignement et de recherche français ou étrangers, des laboratoires publics ou privés.

**Search for the Standard Model Higgs boson
in e^+e^- collisions at \sqrt{s} up to 202 GeV**

L3 Collaboration

Abstract

The Standard Model Higgs boson is searched for in 233.2 pb^{-1} of data collected by the L3 detector at centre of mass energies from 192 GeV to 202 GeV. These data are consistent with the expectations of Standard Model processes and no evidence of a Higgs signal is observed. A lower limit on the mass of the Standard Model Higgs boson of 107.0 GeV is set at the 95% confidence level.

Submitted to *Phys. Lett. B*

1 Introduction

The Standard Model of the electroweak interactions [1] contains a single Higgs doublet [2] which gives rise to a neutral scalar particle, the Higgs boson. Its mass, m_H , is a free parameter of the theory. A global fit to electroweak precision measurements results in an upper limit on m_H of 133 GeV [3] at 95% confidence level (CL). Results of SM Higgs boson searches in e^+e^- collisions were published up to centre of mass energies of 189 GeV in the Higgs mass range up to 95.3 GeV by L3 [4] and by other LEP experiments [5].

In this paper, the results of a Higgs search performed on the data sample collected by L3 at \sqrt{s} up to 202 GeV are reported. The dominant Higgs production mode is

$$e^+e^- \rightarrow Z^* \rightarrow HZ .$$

The processes of W^+W^- and ZZ fusion, which contribute with smaller rate to the Higgs production in the $H\nu\bar{\nu}$ and $H\ell^+\ell^-$ channels, respectively, are also considered. All significant Higgs decay modes are considered in the search. The largest sources of background are four-fermion final states from W and Z pair production, as well as $e^+e^- \rightarrow q\bar{q}(\gamma)$.

2 Data and Monte Carlo samples

The data were collected using the L3 detector [6] at LEP during the year 1999. The integrated luminosities are 29.7 pb^{-1} at $\sqrt{s} = 191.6 \text{ GeV}$, 83.7 pb^{-1} at $\sqrt{s} = 195.5 \text{ GeV}$, 82.8 pb^{-1} at $\sqrt{s} = 199.5 \text{ GeV}$ and 37.0 pb^{-1} at $\sqrt{s} = 201.8 \text{ GeV}$.

The Higgs production cross sections and branching ratios are calculated using the HZHA generator [7]. Efficiencies are determined on Monte Carlo samples of Higgs events, generated using PYTHIA [8]. Standard Model background estimates rely on the following Monte Carlo programs: PYTHIA ($e^+e^- \rightarrow q\bar{q}(\gamma)$ and $e^+e^- \rightarrow Ze^+e^-$), KORALW [9] ($e^+e^- \rightarrow W^+W^-$), KORALZ [10] ($e^+e^- \rightarrow \tau^+\tau^-$), PHOJET [11] ($e^+e^- \rightarrow e^+e^-q\bar{q}$) and EXCALIBUR [12] for other four fermion final states. The number of simulated events for the dominant backgrounds is at least 100 times the number of collected data events for such processes. For the Higgs signals, at least 2000 events are simulated for each search channel and for several masses. Higgs events are simulated with m_H between 95 and 110 GeV, with a step of 1 GeV. Events for Higgs masses between 50 and 95 GeV are simulated with a step of 5 GeV.

The response of the L3 detector is simulated using the GEANT program [13], taking into account the effects of multiple scattering, energy loss and showering in the detector. Hadronic interactions in the detector are modelled using the GHEISHA program [14]. Time dependent detector inefficiencies, as monitored during the data taking period, are also simulated.

3 Analysis procedures

The search for the Standard Model Higgs boson is based on the study of four distinct event topologies representing approximately 98% of the HZ decay modes: $q\bar{q}q\bar{q}$, $q\bar{q}\nu\bar{\nu}$, $q\bar{q}\ell^+\ell^-$ ($\ell = e, \mu, \tau$) and $\tau^+\tau^-q\bar{q}$. With the exception of the $HZ \rightarrow \tau^+\tau^-q\bar{q}$ decay mode, all the analyses are optimised for $H \rightarrow b\bar{b}$ decay. This mode represents about 82% of the Higgs branching fraction in the mass range of interest.

All these channels are analysed in three stages. First, a high multiplicity hadronic event selection, preserving most of the Higgs signal, is applied to reduce the large background from

two-photon processes. In a second stage, a cut based analysis is applied to the $q\bar{q}q\bar{q}$ and lepton topologies, while a neural network based analysis is used for the $q\bar{q}\nu\bar{\nu}$ final states. All the analyses use topological and kinematical variables, which are not strongly dependent on the Higgs mass. B hadrons are identified on the basis of an event b-tag variable, obtained as a combination of the b-tag for each hadronic jet [15]. A neural network is used to calculate the b-tag for each hadronic jet from the three-dimensional decay lengths, properties of semileptonic b decays and jet-shape variables. The third part of the analysis is the construction of a final discriminant for each topology. This is built from a combination of the event b-tag variable and the reconstructed Higgs mass, for the cut based analyses. For the neural network based analysis, it is a combination of the neural network output with the reconstructed Higgs mass. The distributions of the final discriminants are computed for the data, for the expected background and signals for each Higgs mass hypothesis.

4 The $HZ \rightarrow b\bar{b}q\bar{q}$ selection

The selection aims to single out events with four jets, two of which contain b hadrons, while the invariant mass of the other two must be consistent with the Z mass, m_Z . Background from Standard Model processes comes mainly from $q\bar{q}$ final states with hard gluons, W^+W^- and ZZ events, especially those where one of the Z bosons decays into b quarks.

A preselection to accept high multiplicity hadronic events is applied. The retained events are forced into four jets with the DURHAM algorithm [16]. Then a kinematic fit requiring 4-momentum conservation is performed.

In order to differentiate the Higgs signal from background, selection criteria mainly based on kinematic variables, are chosen to maximise the expected performance of the analysis [4]. The quantities used for the selection are: the dijet masses, the minimum jet energy, the maximum energy difference between any two jets, the parameter of the DURHAM scheme for which the event is resolved from three jets into four jets, Y_{34}^D , and the number of charged tracks. The consistency of the dijet masses with a given m_H hypothesis is quantified by a χ^2 -probability that depends on m_H and m_Z [4]. Only a loose cut is placed on this variable.

After these cuts, about 85% of the expected background comes from W^+W^- events. These are characterised by their low b-tag values and by dijet masses close to the W mass. The remaining events are then split for the final analysis into a high purity and a low purity sample according to the value of the reconstructed dijet mass, M_{eq}^{5C} . This is calculated with a five constraints kinematic fit where equal masses are assumed for the two dijet systems. The event is assigned to the high purity sample if $M_{\text{eq}}^{5C} > a \times m_H + b$, or to the low purity sample otherwise. The quantities a and b are optimised for each centre of mass energy. Typical values are $a \sim 0.6$ and $b \sim 40$ GeV. The low purity sample contains most of the properly reconstructed W^+W^- events. Loose b-tag cuts are applied in the final selection and they are separately optimised at each centre of mass energy for the two samples. They are tighter for the low purity one.

The low purity sample contains 109 events with 108 expected from background, corresponding to an efficiency of about 28% for $HZ \rightarrow b\bar{b}q\bar{q}$ and $m_H = 105$ GeV. The high purity sample contains 32 events with 40 expected from background, corresponding to an efficiency of about 30% for a Higgs mass of 105 GeV.

The final discriminant is then calculated as the weighted probability [4] that an event is consistent with the background distributions of both the b-tag and the mass variable. This weighted probability depends on the mass hypothesis and the discriminant is calculated for each test mass. The b-tag, the mass χ^2 and the final discriminant distributions for all the events in

the low purity and high purity samples are shown in Figure 1 for a Higgs mass hypothesis of 105 GeV. A good agreement between the data and the expected background is observed in all the distributions.

5 The $\text{HZ} \rightarrow \text{b}\bar{\text{b}}\nu\bar{\nu}$ selection

This selection searches for events with two acoplanar jets containing b hadrons, with large missing energy and with missing mass consistent with m_Z .

In the first step, high multiplicity hadronic events are selected. The events are forced into two jets using the DURHAM algorithm. The dijet invariant mass must exceed 40 GeV. These requirements reduce contributions from purely leptonic two fermion final states, as well as two-photon interactions, while retaining a significant fraction of hadronic events from $e^+e^- \rightarrow q\bar{q}(\gamma)$ and W-pair production. These backgrounds are further reduced by requiring the visible mass to be less than 120 GeV and the mass recoiling against the hadronic system to lie between 50 GeV and 130 GeV.

Events from $e^+e^- \rightarrow q\bar{q}(\gamma)$ are further suppressed by requiring the longitudinal missing energy to be less than $0.7\sqrt{s}$, the missing energy transverse to the beam axis to be greater than 5 GeV and the missing momentum vector to be at least 16° away from this axis. The energy in the forward luminosity calorimeter is required to be smaller than 15 GeV. The opening angle between the two jets has to be greater than 69° and the angle between the dijet plane and the beam-axis must be greater than 3° . The b-tag distribution, after the above mentioned cuts for all centre of mass energies, is shown in Figure 2a.

An additional cut is applied requiring the event b-tag to be larger than 0.5. After this set of cuts, there are 172 events in the data, while 149 are expected from background processes. The efficiency for $\text{HZ} \rightarrow \text{b}\bar{\text{b}}\nu\bar{\nu}$ with $m_H = 105$ GeV is 62%.

A kinematic fit imposing 4-momentum conservation and requiring the missing mass to be m_Z is performed to compute the hadronic mass. The distribution of this variable is shown in Figure 2b. The output of a mass independent neural network [4] is then combined with the hadronic mass to build the final discriminant. The distribution of the neural network output is shown in Figure 2c. The final discriminant is presented in Figure 2d for the mass hypothesis $m_H = 105$ GeV. The observed data in the $\text{HZ} \rightarrow \text{b}\bar{\text{b}}\nu\bar{\nu}$ analysis are compatible with the background expectations.

6 The $\text{HZ} \rightarrow \text{b}\bar{\text{b}}e^+e^-$ and $\text{HZ} \rightarrow \text{b}\bar{\text{b}}\mu^+\mu^-$ selections

The signatures for the $\text{HZ} \rightarrow \text{b}\bar{\text{b}}e^+e^-$ and $\text{HZ} \rightarrow \text{b}\bar{\text{b}}\mu^+\mu^-$ processes are a pair of high energy electrons or muons, with an invariant mass compatible with m_Z and two hadronic jets with b quark content.

A high multiplicity selection is applied, also requiring two well identified electrons or muons. The visible energy must be larger than $0.7\sqrt{s}$ for the electron analysis and $0.4\sqrt{s}$ for the muon analysis. In the $\text{HZ} \rightarrow \text{b}\bar{\text{b}}e^+e^-$ analysis, the lepton pair must have an opening angle greater than 100° , reduced to 90° in the $\text{HZ} \rightarrow \text{b}\bar{\text{b}}\mu^+\mu^-$ case. Moreover, in the $\text{HZ} \rightarrow \text{b}\bar{\text{b}}e^+e^-$ channel the opening angle between the two jets must be at least 50° . The ratio between the transverse missing momentum and the visible energy should be less than 0.2 in the $\text{HZ} \rightarrow \text{b}\bar{\text{b}}e^+e^-$ channel and less than 0.4 in the $\text{HZ} \rightarrow \text{b}\bar{\text{b}}\mu^+\mu^-$ channel. The value of Y_{34}^D must be larger than 0.0009. Finally, the invariant mass of the leptons after a kinematic fit imposing 4-momentum

conservation must be between 60 GeV and 110 GeV for the electrons and 50 GeV and 125 GeV for the muons.

In the electron channel, 22 events are selected with 20.2 expected from the background and with a signal efficiency of 76% for a Higgs signal of 105 GeV. In the muon channel there are 13 events with 9.2 expected from the background, with a signal efficiency of 56%.

A kinematic fit that requires 4-momentum conservation and constrains the mass of the leptons to m_Z is performed. The dijet mass after this fit is combined with the b-tag values of the two jets, to form the final discriminant [4]. The distributions of the discriminant for the electron and muon channels are shown in Figure 3a and 3b respectively, for the data compared to the expected background and a 105 GeV Higgs signal. The data are consistent with the background predictions.

7 The $\text{HZ} \rightarrow \text{b}\bar{\text{b}}\tau^+\tau^-$ and $\text{HZ} \rightarrow \tau^+\tau^-\text{q}\bar{\text{q}}$ selections

The $\text{HZ} \rightarrow \text{b}\bar{\text{b}}\tau^+\tau^-$ and $\text{HZ} \rightarrow \tau^+\tau^-\text{q}\bar{\text{q}}$ processes result in similar final states, partially distinguished by mass and b-tag information. The semileptonic W and Z pair decays constitute the most significant background sources.

Two inclusive selections are performed, one based on tau identification, the particle-based selection, and the other relying more on the event kinematics, the jet-based selection. Events are accepted if they pass either of the two selections.

First, a high multiplicity selection is applied, also requiring a visible energy greater than $0.4\sqrt{s}$. The events are required to have a value of Y_{34}^D larger than 0.0025. Background from $e^+e^- \rightarrow \text{q}\bar{\text{q}}(\gamma)$ is reduced by rejecting events containing photons with energies greater than 40 GeV. The contribution of $W^+W^- \rightarrow \text{q}\bar{\text{q}}\ell\nu$ ($\ell = e, \mu$) is reduced by requiring the energy of electrons and muons to be below 40 GeV.

In the particle-based selection, tau leptons are identified either by their decay into electrons or muons, or as an isolated low-multiplicity jet with 1 or 3 tracks and unit charge. In the jet-based selection, the event is forced into four jets using the DURHAM algorithm. Two of the jets must have less than 4 tracks each. These jets are considered as tau candidates, but at least one of them must coincide within a 3° cone with a tau candidate identified by the particle-based selection. Both tau candidates must be separated from the hadronic jets by at least 25° . Background contamination from fully hadronic W pair decays is reduced by rejecting events where both tau candidates decay into 3 charged particles and by requiring the visible energy to be smaller than $0.95\sqrt{s}$ for the particle-based selection and smaller than $0.9\sqrt{s}$ for the jet-based one. Moreover, in the jet-based selection, the missing momentum vector should be at least 18° from the beam axis, in order to reduce the $\text{q}\bar{\text{q}}(\gamma)$ contamination.

The invariant masses of the ditau and the dijet are obtained from a kinematic fit which imposes 4-momentum conservation. An event qualifies for the $\text{HZ} \rightarrow \text{b}\bar{\text{b}}\tau^+\tau^-$ channel if the ditau mass is consistent with the mass of the Z boson by lying between 70 GeV and 125 GeV. Similarly, an event is assigned to the $\text{HZ} \rightarrow \tau^+\tau^-\text{q}\bar{\text{q}}$ channel if the dijet mass fulfils the same requirement. The opening angle of the taus or jets assigned to the Higgs boson must be larger than 70° . Those assigned to the Z must be at least 100° apart. Events selected by the $\text{HZ} \rightarrow \text{b}\bar{\text{b}}e^+e^-$ and the $\text{HZ} \rightarrow \text{b}\bar{\text{b}}\mu^+\mu^-$ analyses amount to 3% and are not considered here.

In total, 19 events pass either of the tau selections, with 22.3 events expected from background processes. The efficiency is 29% for both $\text{HZ} \rightarrow \text{b}\bar{\text{b}}\tau^+\tau^-$ and $\text{HZ} \rightarrow \tau^+\tau^-\text{q}\bar{\text{q}}$ at $m_H = 105$ GeV.

The discriminant is defined as in the $\text{HZ} \rightarrow \text{b}\bar{\text{b}}\text{e}^+\text{e}^-$ and $\text{HZ} \rightarrow \text{b}\bar{\text{b}}\mu^+\mu^-$ analyses. Events passing both $\text{HZ} \rightarrow \text{b}\bar{\text{b}}\tau^+\tau^-$ and $\text{HZ} \rightarrow \tau^+\tau^-\text{q}\bar{\text{q}}$ selections are assigned to the channel for which the value of this discriminant is higher. This discriminant is used as the final variable for the $\text{HZ} \rightarrow \text{b}\bar{\text{b}}\tau^+\tau^-$ selection. For the $\text{HZ} \rightarrow \tau^+\tau^-\text{q}\bar{\text{q}}$ selection, the mass of the tau pair, calculated by constraining the invariant mass of the two other jets to m_Z , is used as the final discriminant. Distributions of the final discriminants are shown in the Figures 3c and 3d for data, expected background and a 105 GeV Higgs signal. No evidence of a signal appears in either of the tau channels.

8 Combined results

The results of all the previously described analyses are combined together to set a lower limit on the mass of the Standard Model Higgs boson. A combined CL on the absence of a signal is derived from the distributions of final discriminants in a scan over m_{H} from 50 GeV to 110 GeV. The CL is calculated using the technique of References [15, 17], which takes into account the correlated and the statistical errors.

The systematic uncertainties on the signal and background expectations are derived using the same procedure adopted in previous Standard Model Higgs searches [15]. The overall systematic uncertainty is estimated to be 10% on the number of background events and 4% on the number of signal events. The statistical uncertainty on the background arising from the finite number of generated Monte Carlo events is uncorrelated from bin to bin in the final discriminant distributions, and has little effect on the CL. Bins with a signal-to-background ratio below 0.05 are not considered in the calculation of the CL. This cut was chosen to maximise the median CL, as calculated from a large number of Monte Carlo experiments, thereby minimising the degradation of the result due to these systematic and statistical uncertainties. The results of all the analyses after such a signal-to-background cut are summarised in Table 1 for the data, the expected background and for Higgs signals of 100 GeV and 105 GeV. The number of signal events includes cross-efficiencies from other channels, fusion processes and charm and gluonic Higgs decays.

The measured value of the CL as a function of the Standard Model Higgs boson mass in the range $95 \leq m_{\text{H}} \leq 110$ GeV is shown in the Figure 4a, along with the median of the CL distribution as calculated from a large sample of Monte Carlo experiments under the background-only hypothesis. The median CL represents the sensitivity of the analysis and is equal to 95% at $m_{\text{H}} = 105.2$ GeV. The results of L3 Standard Model Higgs searches at lower centre of mass energies [4] are included in the calculation of these confidence levels. Values of m_{H} from 50 GeV to 95 GeV are excluded in the Standard Model with a confidence level greater than 99%.

Figure 4b shows the background confidence level, CL_b . The observed CL_b is the probability to observe a smaller number of events than the one actually observed, for a background-only hypothesis. The expected CL_b for a background-only hypothesis is 0.5. The observed CL_b gives a measure of the consistency of the data with the expected background. The relatively high value of CL_b in the mass region between 96 and 100 GeV reflects a 2.2 sigma excess of data relative to the background predictions in this mass region. This excess is mainly due to few candidates in the $\text{HZ} \rightarrow \text{b}\bar{\text{b}}\text{q}\bar{\text{q}}$ channel and to one candidate in the $\text{HZ} \rightarrow \text{b}\bar{\text{b}}\text{q}\bar{\text{q}}$ channel with a reconstructed Higgs mass of 100.5 GeV. For $m_{\text{H}} = 107$ GeV, where the observed CL falls below 95%, the CL_b is 8%.

The lower limit on the Standard Model Higgs boson mass is set at

$$m_H > 107.0 \text{ GeV at } 95\% \text{ CL.}$$

This new lower limit improves upon and supersedes our previously published results. A similar result from the 192–202 GeV data was reported [18]. Results from the year 2000 LEP run were recently published [19, 20].

Acknowledgements

We acknowledge the efforts of the engineers and technicians who have participated in the construction and maintenance of L3 and express our gratitude to the CERN accelerator divisions for the superb performance of LEP.

References

- [1] S. L. Glashow, Nucl. Phys. **22** (1961) 579; S. Weinberg, Phys. Rev. Lett. **19** (1967) 1264; A. Salam, in Elementary Particle Theory, ed. N. Svartholm, (Almqvist and Wiksell, Stockholm, 1968), p. 367.
- [2] P. W. Higgs, Phys. Lett. **12** (1964) 132; F. Englert and R. Brout, Phys. Rev. Lett. **13** (1964) 321; G. S. Guralnik *et al.*, Phys. Rev. Lett. **13** (1964) 585.
- [3] L3 Collaboration, M. Acciarri *et al.*, Eur. Phys. J. **C16** (2000) 1.
- [4] L3 Collaboration, M. Acciarri *et al.*, Phys. Lett. **B 461** (1999) 376.
- [5] OPAL Collaboration, G. Abbiendi *et al.*, Eur. Phys. J. **C12** (2000) 567; ALEPH Collaboration, R. Barate *et al.*, Preprint CERN-EP/2000-019 (2000); DELPHI Collaboration, P. Abreu *et al.*, Preprint CERN-EP/2000-038 (2000).
- [6] L3 Collaboration, B. Adeva *et al.*, Nucl. Inst. Meth. **A 289** (1990) 35; L3 Collaboration, O. Adriani *et al.*, Phys. Rep. **236** (1993) 1; J. A. Bakken *et al.*, Nucl. Inst. Meth. **A 275** (1989) 81; O. Adriani *et al.*, Nucl. Inst. Meth. **A 302** (1991) 53; B. Adeva *et al.*, Nucl. Inst. Meth. **A 323** (1992) 109; K. Deiters *et al.*, Nucl. Inst. Meth. **A 323** (1992) 162; M. Chemarin *et al.*, Nucl. Inst. Meth. **A 349** (1994) 345; M. Acciarri *et al.*, Nucl. Inst. Meth. **A 351** (1994) 300; G. Basti *et al.*, Nucl. Inst. Meth. **A 374** (1996) 293; A. Adam *et al.*, Nucl. Inst. Meth. **A 383** (1996) 342.
- [7] P. Janot, "The HZHA generator", in "Physics at LEP2", CERN 96-01 (1996) Vol.2, 309..
- [8] PYTHIA versions 5.722 and 6.1 are used.
T. Sjöstrand, Preprint CERN-TH/7112/93 (1993), revised August 1995; Comp. Phys. Comm. **82** (1994) 74; Preprint hep-ph/0001032 (2000)..
- [9] KORALW version 1.33 is used.
S. Jadach *et al.*, Comp. Phys. Comm. **94** (1996) 216;
S. Jadach *et al.*, Phys. Lett. **B 372** (1996) 289.
- [10] KORALZ version 4.02 is used.
S. Jadach, B.F.L. Ward and Z. Wąs, Comp. Phys. Comm. **79** (1994) 503.
- [11] PHOJET version 1.05 is used.
R. Engel, Z. Phys. **C 66** (1995) 203; R. Engel and J. Ranft, Phys. Rev. **D 54** (1996) 4244.
- [12] F.A. Berends, R. Kleiss and R. Pittau, Comp. Phys. Comm. **85** (1995) 437.
- [13] GEANT Version 3.15 is used,
R. Brun *et al.*, Preprint CERN-DD/EE/84-1 (1984), revised 1987..
- [14] H. Fesefeldt, Preprint PITHA 85/02, RWTH Aachen (1985)..
- [15] L3 Collaboration, M. Acciarri *et al.*, Phys. Lett. **B 411** (1997) 373.
- [16] S. Catani *et al.*, Phys. Lett. **B 269** (1991) 432;
S. Bethke *et al.*, Nucl. Phys. **B 370** (1992) 310.

- [17] A. Favara and M. Pieri, Preprint hep-ex/9706016 (1997)..
- [18] ALEPH Collaboration, R. Barate *et al.*, Preprint CERN-EP/2000-131 (2000).
- [19] ALEPH Collaboration, R. Barate *et al.*, Preprint CERN-EP/2000-138 (2000).
- [20] L3 Collaboration, M. Acciarri *et al.*, Preprint CERN-EP/2000-140 (2000).

The L3 Collaboration:

M.Acciarri,²⁶ P.Achard,¹⁹ O.Adriani,¹⁶ M.Aguilar-Benitez,²⁵ J.Alcaraz,²⁵ G.Alemanni,²² J.Allaby,¹⁷ A.Aloisio,²⁸ M.G.Alvigi,²⁸ G.Ambrosi,¹⁹ H.Anderhub,⁴⁸ V.P.Andreev,^{6,36} T.Angelescu,¹² F.Anselmo,⁹ A.Arefiev,²⁷ T.Azemoon,³ T.Aziz,¹⁰ P.Bagnaia,³⁵ A.Bajo,²⁵ L.Baksay,⁴³ A.Balandras,⁴ S.V.Baldew,² S.Banerjee,¹⁰ Sw.Banerjee,⁴ A.Barczyk,^{48,46} R.Barillère,¹⁷ P.Bartalini,²² M.Basile,⁹ N.Batalova,⁴⁵ R.Battiston,³² A.Bay,²² F.Becattini,¹⁶ U.Becker,¹⁴ F.Behner,⁴⁸ L.Bellucci,¹⁶ R.Berbeco,³ J.Berdugo,²⁵ P.Berges,¹⁴ B.Bertucci,³² B.L.Betev,⁴⁸ S.Bhattacharya,¹⁰ M.Biasini,³² A.Biland,⁴⁸ J.J.Blaising,⁴ S.C.Blyth,³³ G.J.Bobbink,² A.Böhm,¹ L.Boldizsar,¹³ B.Borgia,³⁵ D.Bourilkov,⁴⁸ M.Bourquin,¹⁹ S.Braccini,¹⁹ J.G.Branson,⁴⁰ F.Brochu,⁴ A.Buffini,¹⁶ A.Buijs,⁴⁴ J.D.Burger,¹⁴ W.J.Burger,³² X.D.Cai,¹⁴ M.Capell,¹⁴ G.Cara Romeo,⁹ G.Carlino,²⁸ A.M.Cartacci,¹⁶ J.Casaus,²⁵ G.Castellini,¹⁶ F.Cavallari,³⁵ N.Cavallo,³⁷ C.Cecchi,³² M.Cerrada,²⁵ F.Cesaroni,²³ M.Chamizo,¹⁹ Y.H.Chang,⁵⁰ U.K.Chaturvedi,¹⁸ M.Chemarin,²⁴ A.Chen,⁵⁰ G.Chen,⁷ G.M.Chen,²⁰ H.F.Chen,⁷ H.S.Chen,⁷ G.Chiefari,²⁸ L.Cifarelli,³⁹ F.Cindolo,⁹ C.Civinini,¹⁶ I.Clare,¹⁴ R.Clare,³⁸ G.Coignet,⁴ N.Colino,²⁵ S.Costantini,⁵ F.Cotorobai,¹² B.de la Cruz,²⁵ A.Csilling,¹³ S.Cucciarelli,³² T.S.Dai,¹⁴ J.A.van Dalen,³⁰ R.D'Alessandro,¹⁶ R.de Asmundis,²⁸ P.Dégion,¹⁹ A.Degré,⁴ K.Deiters,⁴⁶ D.della Volpe,²⁸ E.Delmeire,¹⁹ P.Denes,³⁴ F.DeNotaristefani,³⁵ A.De Salvo,⁴⁸ M.Diemoz,³⁵ M.Dierckxsens,² D.van Dierendonck,² C.Dionisi,³⁵ M.Dittmar,⁴⁸ A.Dominguez,⁴⁰ A.Doria,²⁸ M.T.Dova,^{18,4} D.Duchesneau,⁴ D.Dufournaud,⁴ P.Duinker,² H.El Mamouni,²⁴ A.Engler,³³ F.J.Eppling,¹⁴ F.C.Erné,² A.Ewers,¹ P.Extermann,¹⁹ M.Fabre,⁴⁶ M.A.Falagan,²⁵ S.Falciano,^{35,17} A.Favara,¹⁷ J.Fay,²⁴ O.Fedin,³⁶ M.Felcini,⁴⁸ T.Ferguson,³³ H.Fesefeldt,¹ E.Fiandrini,³² J.H.Field,¹⁹ F.Filthaut,¹⁷ P.H.Fisher,¹⁴ I.Fisk,⁴⁰ G.Forconi,¹⁴ K.Freudenreich,⁴⁸ C.Furetta,²⁶ Yu.Galaktionov,^{27,14} S.N.Ganguli,¹⁰ P.Garcia-Abia,⁵ M.Gataullin,³¹ S.S.Gau,¹¹ S.Gentile,^{35,17} N.Gheordanescu,¹² S.Giagu,³⁵ Z.F.Gong,²⁰ G.Grenier,²⁴ O.Grimm,⁴⁸ M.W.Gruenewald,⁸ M.Guida,³⁹ R.van Gulik,² V.K.Gupta,³⁴ A.Gurtu,¹⁰ L.J.Gutay,⁴⁵ D.Haas,⁵ A.Hasan,²⁹ D.Hatzifotiadou,⁹ T.Hebbeker,⁸ A.Hervé,¹⁷ P.Hidas,¹³ J.Hirschfelder,³³ H.Hofer,⁴⁸ G.Holzner,⁴⁸ H.Hoorani,³³ S.R.Hou,⁵⁰ Y.Hu,³⁰ I.Iashvili,⁴⁷ B.N.Jin,⁷ L.W.Jones,³ P.de Jong,² I.Josa-Mutuberría,²⁵ R.A.Khan,¹⁸ D.Käfer,¹ M.Kaur,^{18,4} M.N.Kienzle-Focacci,¹⁹ D.Kim,³⁵ J.K.Kim,⁴² J.Kirkby,¹⁷ D.Kiss,¹³ W.Kittel,³⁰ A.Klimentov,^{14,27} A.C.König,³⁰ M.Kopal,⁴⁵ A.Kopp,⁴⁷ V.Koutsenko,^{14,27} M.Kräber,⁴⁸ R.W.Kraemer,³³ W.Krenz,¹ A.Krüger,⁴⁷ A.Kunin,^{14,27} P.Ladron de Guevara,²⁵ I.Laktineh,²⁴ G.Landi,¹⁶ M.Lebeau,¹⁷ A.Lebedev,¹⁴ P.Lebrun,²⁴ P.Lecomte,⁴⁸ P.Lecoq,¹⁷ P.Le Coultre,⁴⁸ H.J.Lee,⁸ J.M.Le Goff,¹⁷ R.Leiste,⁴⁷ P.Levtchenko,³⁶ C.Li,²⁰ S.Likhoded,⁴⁷ C.H.Lin,⁵⁰ W.T.Lin,⁵⁰ F.L.Linde,² L.Lista,²⁸ Z.A.Liu,⁷ W.Lohmann,⁴⁷ E.Longo,³⁵ Y.S.Lu,⁷ K.Lübelsmeyer,¹ C.Luci,^{17,35} D.Luckey,¹⁴ L.Lugnier,²⁴ L.Luminari,³⁵ W.Lustermann,⁴⁸ W.G.Ma,²⁰ M.Maity,¹⁰ L.Malgeri,¹⁷ A.Malinin,¹⁷ C.Maia,²⁵ D.Mangeol,³⁰ J.Mans,³⁴ G.Marian,¹⁵ J.P.Martin,²⁴ F.Marzano,³⁵ K.Mazumdar,¹⁰ R.R.McNeil,⁶ S.Mele,¹⁷ L.Merola,²⁸ M.Meschini,¹⁶ W.J.Metzger,³⁰ M.von der Mey,¹ A.Mihul,¹² H.Milcent,¹⁷ G.Mirabelli,³ J.Mnich,¹ G.B.Mohanty,¹⁰ T.Moulik,¹⁰ G.S.Muanza,²⁴ A.J.M.Muijs,² B.Musicar,⁴⁰ M.Musy,³⁵ M.Napolitano,²⁸ F.Nessi-Tedaldi,⁴⁸ H.Newman,³¹ T.Niessen,¹ A.Nisati,³⁵ H.Nowak,⁴⁷ R.Ofierzynski,⁴⁸ G.Organtini,³⁵ A.Oulianov,²⁷ C.Palomares,²⁵ D.Pandoulas,¹ S.Paoletti,^{35,17} P.Paolucci,²⁸ R.Paramatti,³⁵ H.K.Park,³³ I.H.Park,⁴² G.Passaleva,¹⁷ S.Patricelli,²⁸ T.Paul,¹¹ M.Pauluzzi,³² C.Paus,¹⁷ F.Pauss,⁴⁸ M.Pedace,³⁵ S.Pensotti,²⁶ D.Perret-Gallix,⁴ B.Petersen,³⁰ D.Piccolo,²⁸ F.Pierella,⁹ M.Pieri,¹⁶ P.A.Piroué,³⁴ E.Pistolessi,²⁶ V.Plyaskin,²⁷ M.Pohl,¹⁹ V.Pojidaev,^{27,16} H.Postema,¹⁴ J.Pothier,¹⁷ D.O.Prokofiev,⁴⁵ D.Prokofiev,³⁶ J.Quartieri,³⁹ G.Rahal-Callot,^{48,17} M.A.Rahaman,¹⁰ P.Raics,¹⁵ N.Raja,¹⁰ R.Ramelli,⁴⁸ P.G.Rancoita,²⁶ R.Ranieri,¹⁶ A.Raspereza,⁴⁷ G.Raven,⁴⁰ P.Razis,²⁹ D.Ren,⁴⁸ M.Rescigno,³⁵ S.Reucroft,¹¹ S.Riemann,⁴⁷ K.Riles,³ J.Rodin,⁴³ B.P.Roe,³ L.Romero,²⁵ A.Rosca,⁸ S.Rosier-Lees,⁴ S.Roth,¹ C.Rosenbleck,¹ B.Roux,³⁰ J.A.Rubio,¹⁷ G.Ruggiero,¹⁶ H.Rykaczewski,⁴⁸ S.Saremi,⁶ S.Sarkar,³⁵ J.Salicio,¹⁷ E.Sanchez,¹⁷ M.P.Sanders,³⁰ C.Schäfer,¹⁷ V.Schegelsky,³⁶ S.Schmidt-Kaerst,¹ D.Schmitz,¹ H.Schopper,⁴⁹ D.J.Schotanus,³⁰ G.Schwering,¹ C.Sciacca,²⁸ A.Seganti,⁹ L.Servoli,³² S.Shevchenko,³¹ N.Shivarov,⁴¹ V.Shoutko,²⁷ E.Shumilov,²⁷ A.Shvorob,³¹ T.Siedenburger,¹ D.Son,⁴² B.Smith,³³ P.Spillantini,¹⁶ M.Steuer,¹⁴ D.P.Stickland,³⁴ A.Stone,⁶ B.Stoyanov,⁴¹ A.Straessner,¹ K.Sudhakar,¹⁰ G.Sultanov,¹⁸ L.Z.Sun,²⁰ S.Sushkov,⁸ H.Suter,⁴⁸ J.D.Swain,¹⁸ Z.Szillasi,^{43,4} T.Sztricskai,^{43,4} X.W.Tang,⁷ L.Tauscher,⁵ L.Taylor,¹¹ B.Tellili,²⁴ D.Teyssier,²⁴ C.Timmermans,³⁰ Samuel C.C.Ting,¹⁴ S.M.Ting,¹⁴ S.C.Tonwar,¹⁰ J.Tóth,¹³ C.Tully,¹⁷ K.L.Tung,⁷ Y.Uchida,¹⁴ J.Ulbricht,⁴⁸ E.Valente,³⁵ G.Vesztergombi,¹³ I.Vetlitsky,²⁷ D.Vicinanza,³⁹ G.Viertel,⁴⁸ S.Villa,¹¹ M.Vivargent,⁴ S.Vlachos,⁵ I.Vodopianov,³⁶ H.Vogel,³³ H.Vogt,⁴⁷ I.Vorobiev,³³ A.A.Vorobyov,³⁶ A.Vorvolakos,²⁹ M.Wadhwa,⁵ W.Wallraff,¹ M.Wang,¹⁴ X.L.Wang,²⁰ Z.M.Wang,²⁰ A.Weber,¹ M.Weber,¹ P.Wienemann,¹ H.Wilkens,³⁰ S.X.Wu,¹⁴ S.Wynhoff,¹⁷ L.Xia,³¹ Z.Z.Xu,²⁰ J.Yamamoto,³ B.Z.Yang,²⁰ C.G.Yang,⁷ H.J.Yang,⁷ M.Yang,⁷ J.B.Ye,²⁰ S.C.Yeh,⁵¹ An.Zalite,³⁶ Yu.Zalite,³⁶ Z.P.Zhang,²⁰ G.Y.Zhu,⁷ R.Y.Zhu,³¹ A.Zichichi,^{9,17,18} G.Zilizi,^{43,4} B.Zimmermann,⁴⁸ M.Zöller.¹

- 1 I. Physikalisches Institut, RWTH, D-52056 Aachen, FRG[§]
III. Physikalisches Institut, RWTH, D-52056 Aachen, FRG[§]
 - 2 National Institute for High Energy Physics, NIKHEF, and University of Amsterdam, NL-1009 DB Amsterdam, The Netherlands
 - 3 University of Michigan, Ann Arbor, MI 48109, USA
 - 4 Laboratoire d'Annecy-le-Vieux de Physique des Particules, LAPP, IN2P3-CNRS, BP 110, F-74941 Annecy-le-Vieux CEDEX, France
 - 5 Institute of Physics, University of Basel, CH-4056 Basel, Switzerland
 - 6 Louisiana State University, Baton Rouge, LA 70803, USA
 - 7 Institute of High Energy Physics, IHEP, 100039 Beijing, China[△]
 - 8 Humboldt University, D-10099 Berlin, FRG[§]
 - 9 University of Bologna and INFN-Sezione di Bologna, I-40126 Bologna, Italy
 - 10 Tata Institute of Fundamental Research, Bombay 400 005, India
 - 11 Northeastern University, Boston, MA 02115, USA
 - 12 Institute of Atomic Physics and University of Bucharest, R-76900 Bucharest, Romania
 - 13 Central Research Institute for Physics of the Hungarian Academy of Sciences, H-1525 Budapest 114, Hungary[‡]
 - 14 Massachusetts Institute of Technology, Cambridge, MA 02139, USA
 - 15 KLTE-ATOMKI, H-4010 Debrecen, Hungary[¶]
 - 16 INFN Sezione di Firenze and University of Florence, I-50125 Florence, Italy
 - 17 European Laboratory for Particle Physics, CERN, CH-1211 Geneva 23, Switzerland
 - 18 World Laboratory, FBLJA Project, CH-1211 Geneva 23, Switzerland
 - 19 University of Geneva, CH-1211 Geneva 4, Switzerland
 - 20 Chinese University of Science and Technology, USTC, Hefei, Anhui 230 029, China[△]
 - 22 University of Lausanne, CH-1015 Lausanne, Switzerland
 - 23 INFN-Sezione di Lecce and Università Degli Studi di Lecce, I-73100 Lecce, Italy
 - 24 Institut de Physique Nucléaire de Lyon, IN2P3-CNRS, Université Claude Bernard, F-69622 Villeurbanne, France
 - 25 Centro de Investigaciones Energéticas, Medioambientales y Tecnológicas, CIEMAT, E-28040 Madrid, Spain^b
 - 26 INFN-Sezione di Milano, I-20133 Milan, Italy
 - 27 Institute of Theoretical and Experimental Physics, ITEP, Moscow, Russia
 - 28 INFN-Sezione di Napoli and University of Naples, I-80125 Naples, Italy
 - 29 Department of Natural Sciences, University of Cyprus, Nicosia, Cyprus
 - 30 University of Nijmegen and NIKHEF, NL-6525 ED Nijmegen, The Netherlands
 - 31 California Institute of Technology, Pasadena, CA 91125, USA
 - 32 INFN-Sezione di Perugia and Università Degli Studi di Perugia, I-06100 Perugia, Italy
 - 33 Carnegie Mellon University, Pittsburgh, PA 15213, USA
 - 34 Princeton University, Princeton, NJ 08544, USA
 - 35 INFN-Sezione di Roma and University of Rome, "La Sapienza", I-00185 Rome, Italy
 - 36 Nuclear Physics Institute, St. Petersburg, Russia
 - 37 INFN-Sezione di Napoli and University of Potenza, I-85100 Potenza, Italy
 - 38 University of California, Riverside, CA 92521, USA
 - 39 University and INFN, Salerno, I-84100 Salerno, Italy
 - 40 University of California, San Diego, CA 92093, USA
 - 41 Bulgarian Academy of Sciences, Central Lab. of Mechatronics and Instrumentation, BU-1113 Sofia, Bulgaria
 - 42 Laboratory of High Energy Physics, Kyungpook National University, 702-701 Taegu, Republic of Korea
 - 43 University of Alabama, Tuscaloosa, AL 35486, USA
 - 44 Utrecht University and NIKHEF, NL-3584 CB Utrecht, The Netherlands
 - 45 Purdue University, West Lafayette, IN 47907, USA
 - 46 Paul Scherrer Institut, PSI, CH-5232 Villigen, Switzerland
 - 47 DESY, D-15738 Zeuthen, FRG
 - 48 Eidgenössische Technische Hochschule, ETH Zürich, CH-8093 Zürich, Switzerland
 - 49 University of Hamburg, D-22761 Hamburg, FRG
 - 50 National Central University, Chung-Li, Taiwan, China
 - 51 Department of Physics, National Tsing Hua University, Taiwan, China
- § Supported by the German Bundesministerium für Bildung, Wissenschaft, Forschung und Technologie
‡ Supported by the Hungarian OTKA fund under contract numbers T019181, F023259 and T024011.
¶ Also supported by the Hungarian OTKA fund under contract numbers T22238 and T026178.
^b Supported also by the Comisión Interministerial de Ciencia y Tecnología.
[‡] Also supported by CONICET and Universidad Nacional de La Plata, CC 67, 1900 La Plata, Argentina.
[△] Also supported by Panjab University, Chandigarh-160014, India.
[△] Supported by the National Natural Science Foundation of China.

$\sqrt{s} = 192$ GeV		Mass hypothesis					
Selection		$m_H = 100$ GeV			$m_H = 105$ GeV		
H	Z	N_D	N_B	N_S	N_D	N_B	N_S
$b\bar{b}$	$q\bar{q}$	4	2.9	0.5	0	0.2	0.0
$b\bar{b}$	$\nu\bar{\nu}$	1	1.8	0.2	0	0.1	0.0
$b\bar{b}$	e^+e^-	0	0.1	0.1	0	0.0	0.0
$b\bar{b}$	$\mu^+\mu^-$	1	0.1	0.0	0	0.1	0.0
$b\bar{b}$	$\tau^+\tau^-$	0	0.0	0.0	0	0.0	0.0
$\tau^+\tau^-$	$q\bar{q}$	0	0.1	0.0	0	0.0	0.0
Total		6	5.0	0.8	0	0.4	0.0

$\sqrt{s} = 196$ GeV		Mass hypothesis					
Selection		$m_H = 100$ GeV			$m_H = 105$ GeV		
H	Z	N_D	N_B	N_S	N_D	N_B	N_S
$b\bar{b}$	$q\bar{q}$	31	28.2	5.2	6	5.2	0.7
$b\bar{b}$	$\nu\bar{\nu}$	4	6.9	1.7	0	1.3	0.2
$b\bar{b}$	e^+e^-	1	0.7	0.4	0	0.2	0.0
$b\bar{b}$	$\mu^+\mu^-$	1	0.6	0.3	1	0.2	0.0
$b\bar{b}$	$\tau^+\tau^-$	0	0.2	0.1	1	0.1	0.0
$\tau^+\tau^-$	$q\bar{q}$	1	0.3	0.3	0	0.1	0.0
Total		38	36.9	8.0	9	7.1	0.9

$\sqrt{s} = 200$ GeV		Mass hypothesis					
Selection		$m_H = 100$ GeV			$m_H = 105$ GeV		
H	Z	N_D	N_B	N_S	N_D	N_B	N_S
$b\bar{b}$	$q\bar{q}$	24	29.9	6.9	18	18.2	3.6
$b\bar{b}$	$\nu\bar{\nu}$	13	8.6	2.2	4	3.6	1.1
$b\bar{b}$	e^+e^-	3	1.2	0.5	1	1.0	0.2
$b\bar{b}$	$\mu^+\mu^-$	0	0.8	0.4	0	0.4	0.2
$b\bar{b}$	$\tau^+\tau^-$	0	0.5	0.2	0	0.2	0.1
$\tau^+\tau^-$	$q\bar{q}$	0	0.9	0.4	0	0.5	0.1
Total		40	41.9	10.6	23	23.9	5.3

$\sqrt{s} = 202$ GeV		Mass hypothesis					
Selection		$m_H = 100$ GeV			$m_H = 105$ GeV		
H	Z	N_D	N_B	N_S	N_D	N_B	N_S
$b\bar{b}$	$q\bar{q}$	13	12.5	3.0	7	8.5	2.0
$b\bar{b}$	$\nu\bar{\nu}$	6	2.5	1.0	4	2.7	0.7
$b\bar{b}$	e^+e^-	0	0.5	0.2	0	0.6	0.1
$b\bar{b}$	$\mu^+\mu^-$	0	0.4	0.2	0	0.2	0.1
$b\bar{b}$	$\tau^+\tau^-$	0	0.2	0.1	0	0.1	0.1
$\tau^+\tau^-$	$q\bar{q}$	0	0.4	0.2	0	0.3	0.1
Total		19	16.5	4.7	11	12.4	3.1

Table 1: The number of observed candidates (N_D), expected background events (N_B) and expected signal (N_S) for the $\sqrt{s} = 192$ GeV, 196 GeV, 200 GeV, 202 GeV data after a cut on the final discriminant corresponding to a signal-to-background ratio greater than 0.05. This cut is used to calculate the confidence levels.

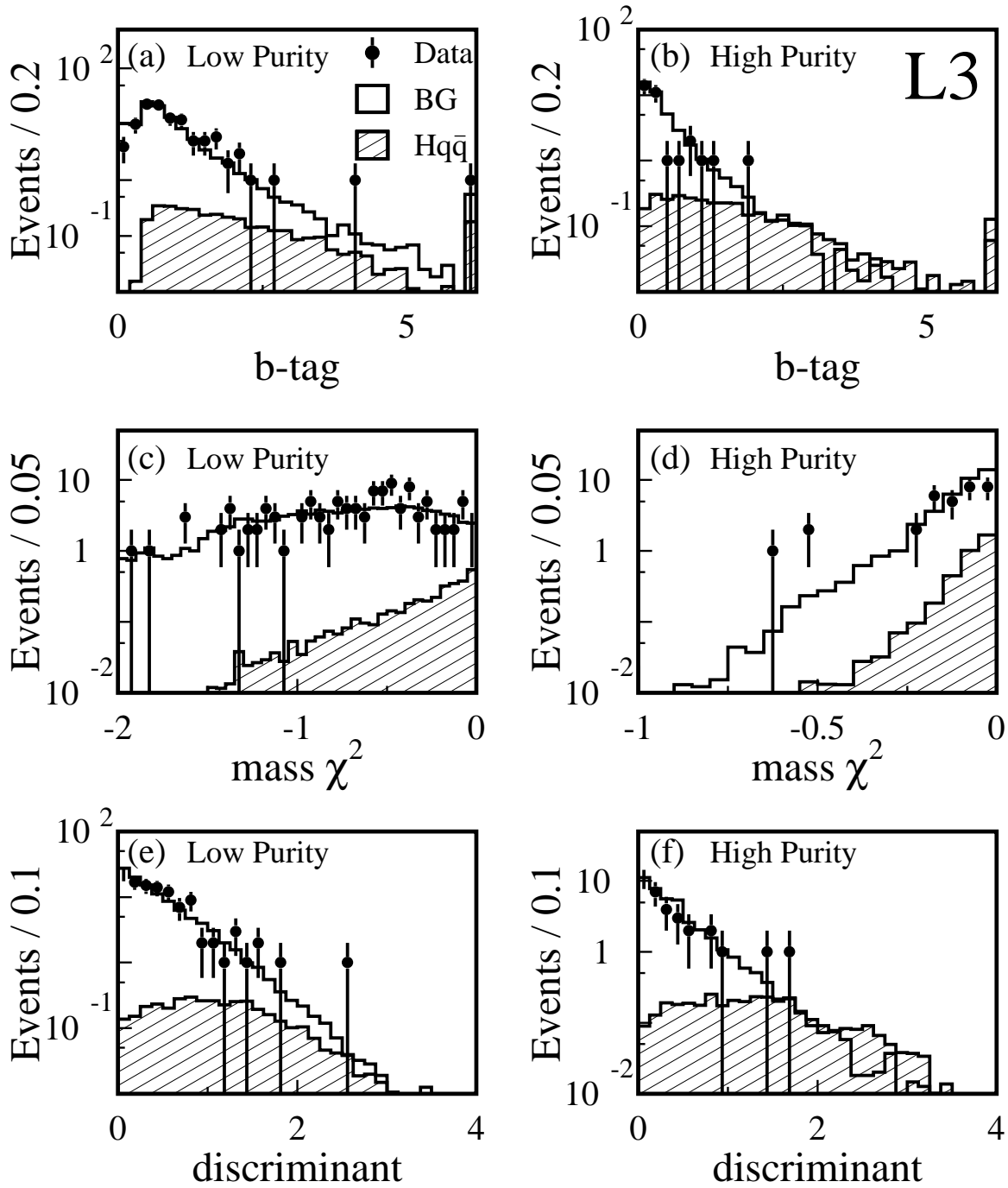


Figure 1: The b-tag (a and b), the mass χ^2 (c and d) and the final discriminant (e and f) distributions for the low purity and high purity $\text{HZ} \rightarrow \text{bb}\bar{\text{q}}\bar{\text{q}}$ selections. The points are the 192–202 GeV data, the open histograms are the expected background and the hatched histograms are the expected Higgs signal from the $\text{HZ} \rightarrow \text{bb}\bar{\text{q}}\bar{\text{q}}$ channel with $m_{\text{H}} = 105$ GeV. The last bin on the right of the b-tag distributions groups the overflows.

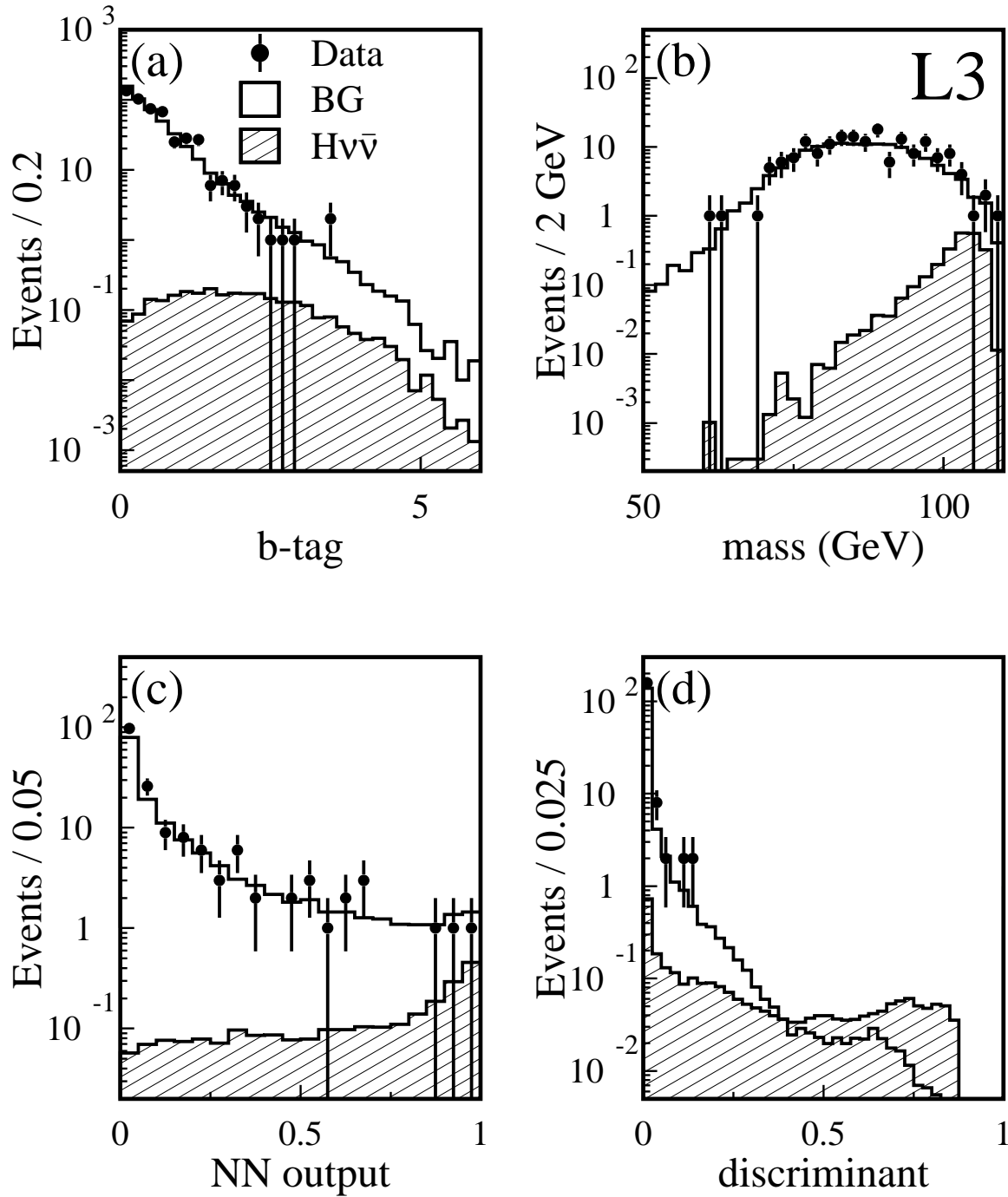


Figure 2: Distributions of (a) b-tag, (b) hadronic mass (c) neural network output and (d) final discriminant for the $HZ \rightarrow b\bar{b}\nu\bar{\nu}$ selection. The points are the 192–202 GeV data, the open histograms are the expected background and the hatched histograms the $HZ \rightarrow b\bar{b}\nu\bar{\nu}$ expected signal with $m_H = 105$ GeV.

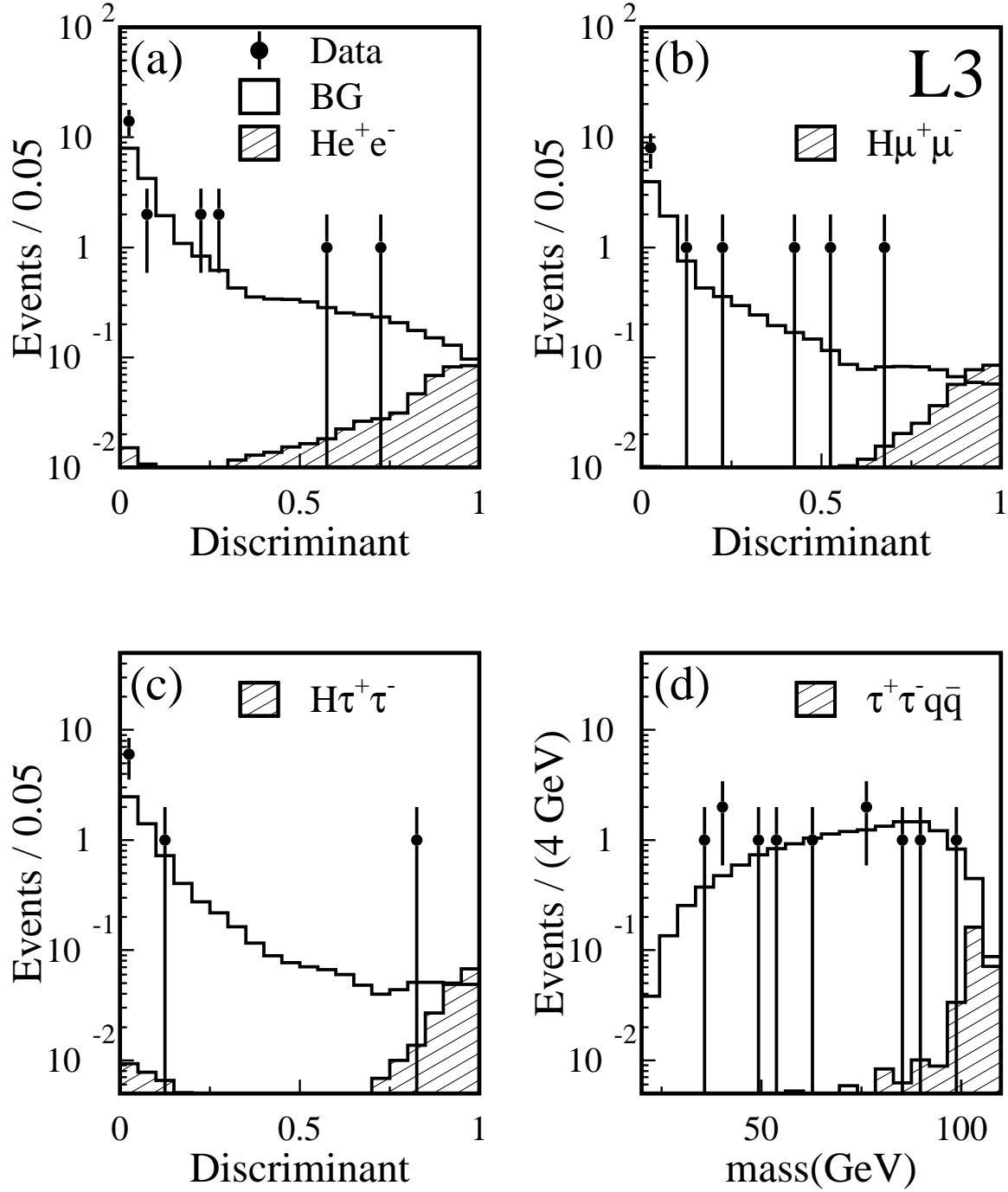


Figure 3: Distributions of the final discriminant for the (a) $HZ \rightarrow b\bar{b}e^+e^-$, (b) $HZ \rightarrow b\bar{b}\mu^+\mu^-$, (c) $HZ \rightarrow b\bar{b}\tau^+\tau^-$ and (d) $HZ \rightarrow \tau^+\tau^-q\bar{q}$ selections. The 192–202 GeV data (points) are compared to the expected background (open histogram) and to the expected Higgs signal (hatched histogram) of 105 GeV. The signal events in the $HZ \rightarrow b\bar{b}\tau^+\tau^-$ and $HZ \rightarrow \tau^+\tau^-q\bar{q}$ distributions include the cross-efficiencies for these channels. Events are uniquely assigned to only one of these channels.

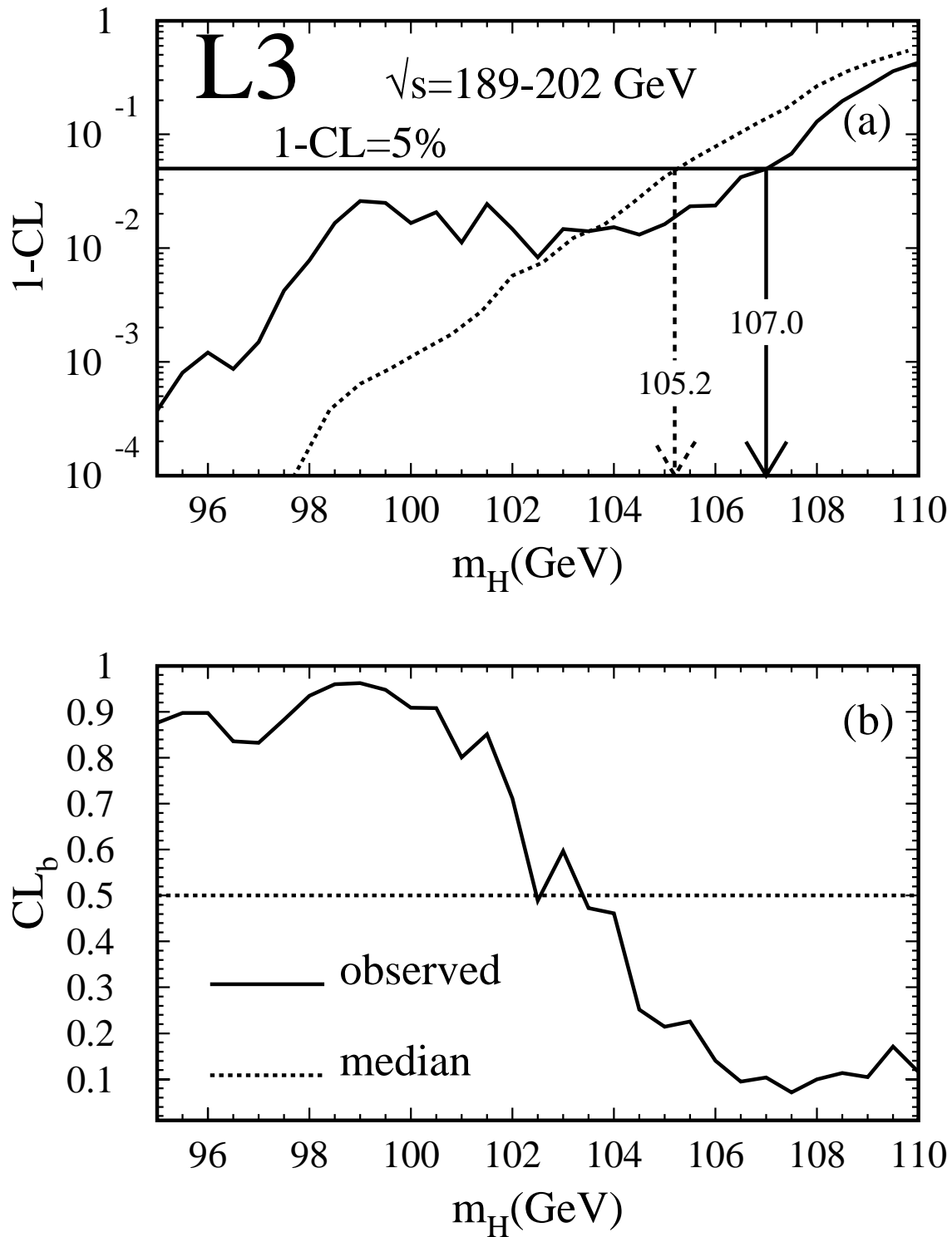


Figure 4: (a) The observed (solid line) and expected median (dashed line) signal confidence levels ($1-CL$) as a function of the Higgs mass, (b) the observed (solid line) and expected (dashed line) background confidence level CL_b as a function of the Higgs mass. The lower limit on the Higgs mass is set at 107.0 GeV at the 95% CL.